ACS OMEGA

Open Access

http://pubs.acs.org/journal/acsodf

Article

Synergistic Combination of Dual Clays in Multilayered Nanocomposites for Enhanced Flame Retardant Properties

Inyoung Lee,[#] Jinhong Kim,[#] Sehui Yun, Junho Jang, Se Youn Cho, Jung Sang Cho, Ji Hyun Ryu,* Dongwhi Choi,* and Chungyeon Cho*

Cite This: *ACS Omega* 2024, 9, 6606−6615

Read Online

ACCESS | Metrics & More | Article Recommendations | Supporting Information

ABSTRACT: In an effort to reduce the flammability of synthetic polymeric materials such as cotton fabrics and polyurethane foam (PUF), hybrid nanocoatings are prepared by layer-by-layer assembly. Multilayered nanocomposites of a cationic polyelectrolyte, poly(diallyldimethylammonium chloride) (PDDA), are paired with two kinds of clay nanoplatelets, montmorillonite (MMT) and vermiculite (VMT). The physical properties such as thickness and mass and thermal behaviors in clay-based nanocoatings with and without incorporation of tris buffer are compared to assess the effectiveness of amine salts on flame retardant (FR) performances. A PDDA-tris/VMT-MMT system, in which tris buffer is introduced into the cationic PDDA aqueous solution, produces a thicker and heavier coating. Three different systems, including PDDA/MMT, PDDA/VMT-MMT, and PDDA-tris/VMT-MMT, result in conformal coating, retaining the weave structure of the fabrics after being exposed to a vertical and horizontal flame test, while the uncoated sample is completely burned out. The synergistic effects of dual clay-based hybrid nanocoatings are greatly improved by adding amine salts. Cone calorimetry reveals that the PDDA-tris/VMT-MMT-coated PUF eliminates a second peak heat release rate and significantly reduces other FR performances, compared to those obtained from the clay-based multilayer films with no amine salts added. Ten bilayers of PDDA-tris/VMT-MMT (≈250 nm thick) maintain the shape of foam after exposure to a butane torch flame for 12 s. As for practical use of these nanocomposites in real fire disasters, spray-assisted PDDA-tris/VMT-MMT multilayers on woods exhibit high resistance over flammability. Improved fire resistance in PDDA-tris/VMT-MMT is believed to be due to the enhanced char yield through the addition of tris buffer that promotes the deposition of more clay particles while retaining a highly ordered deposition of a densely packed nanobrick wall structure. This work demonstrates the ability to impart significant fire resistance to synthetic polymer materials in a fully renewable nanocoating that uses environmentally benign chemistry.

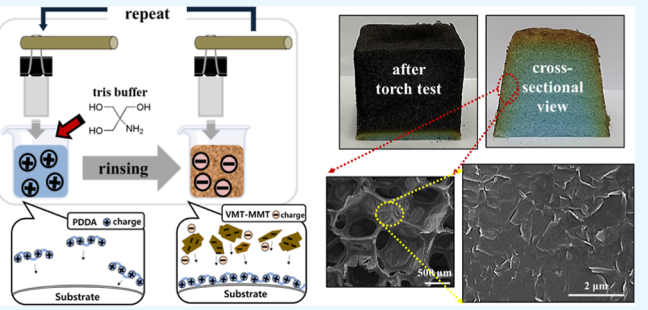

INTRODUCTION

Due to their excellent electrical insulating properties, the ability to be recycled, and good chemical stability, synthetic polymer-based materials such as textile fibers and polyurethane foams (PUF) have been commercially applied in a great variety of industrial applications, including furniture, transportation, and aerospace.[1,2] However, these synthetic polymers with no flame retardant (FR) additives possess high combustibility and emit a large amount of toxic gases due to their organic nature, high permeability to air, and high specific surface areas, which impedes the practical applications in many areas where high thermal protection is necessary.[3] Halogenated compounds have been the most commonly used FRs, owing to their high retardancy, low cost, and ease of processability. However, growing concerns with regard to potential threats to human health and adverse impacts on environmental persistence have prompted significant research into the development of an environmentally benign alternative.[4,5]

Clay nanoplatelets as the phyllosilicate minerals group have been investigated extensively for many applications due to their unique structure, thermal resistance, barrier properties, mechanical strength, and natural abundance.[6−9] Among various clays, montmorillonite (MMT) and vermiculite (VMT) have been widely reported to be environmentally benign alternatives, replacing halogen-based compounds in FR applications, thanks to their high char-forming character.[10,11] The hybrids of these clays with a high-aspect-ratio layered structure into a polymer matrix have been shown to be effective in reducing the heat release rate (HRR) during the combustion process. Various strategies have been developed to

Received: September 29, 2023
Revised: January 9, 2024
Accepted: January 12, 2024
Published: January 31, 2024

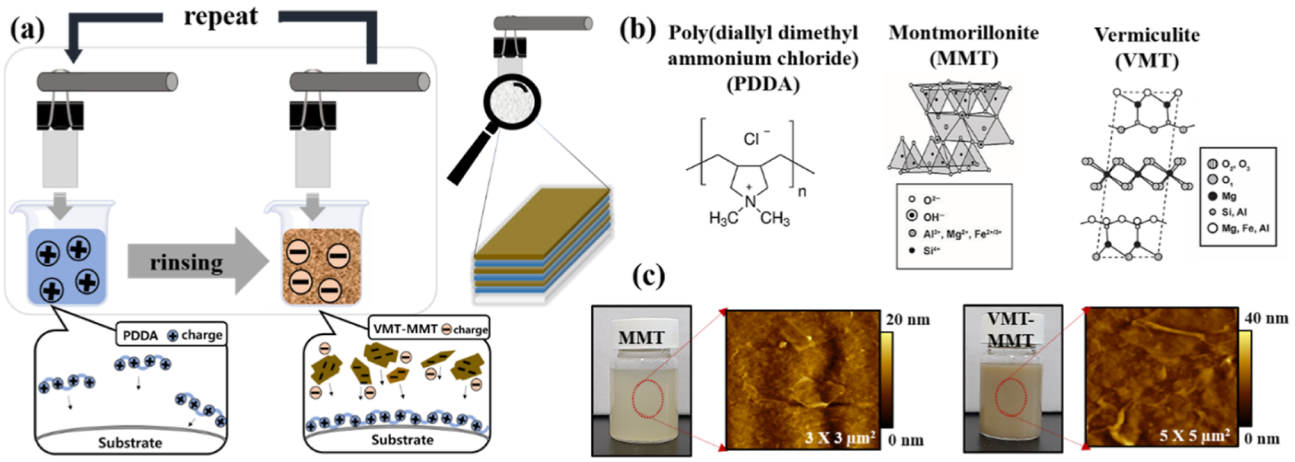

Figure 1. (a) Schematic of construction of LbL thin films, (b) chemical structures used in this study (reproduced with permission for an MMT structure from Morgan A. Priolo et al. Copyright 2015, WIELY-VCH and for a VMT structure from Long et al. Copyright 2022, Springer Nature),[35,36] and (c) photo images of MMT and VMT-MMT suspensions and corresponding AFM images.

date in the preparation of clay-based polymer nanocomposites using simple mixing, melt intercalation, in situ polymerization, and template synthesis.[12−14] In order to fully realize the synergistic combination of clay sheets in the polymer nanocomposites, it is highly required for nanofillers to be uniformly deposited with a networked structure. However, difficulties in precise control of film architecture and the low compatibility of nanoplatelets in polymer matrix prevent the reinforcement of properties in clay-based nanocomposites.

The layer-by-layer (LbL) technique has proven to be a versatile, cost-effective, and powerful means for creating multifunctional polymer coatings with exceptional properties because of its simplicity, low cost, the use of water-based solutions, and ease of controlling the template's thickness.[15−18] The coating procedure consists of subsequent deposition of various species with complementary functionality onto solid substrates, which leads to the assembly of a multilayered film. LbL assembly is mainly driven by electrostatic attractions, but other molecular interactions, such as hydrogen bonding, donor/acceptor interactions, molecular recognition, charge transfer, and hydrophobic interaction have been also widely exploited for LbL deposition.[19−22] Surface charge reversal after each adsorption process controls the growth behavior and prepares the surface to adsorb the subsequent adsorption of the oppositely charged polyelectrolyte.[23] The thickness of each individual layer is typically 1−100 nm and can be precisely controlled on the nanoscale level by tailoring the processing conditions such as assembly pH conditions of the species being deposited, counterions, molecular weight, ionic strength, and temperature.[24−26] The LbL technology has been utilized to produce multilayered functional materials for many research fields that include antimicrobial/antireflective surfaces, electrodes for electrochemical energy storage, biomedical applications, and electronic devices.[27−30]

The aim of the present study is to investigate the synergistic potential effects of the addition of tris buffer (a common amine salt) into a cationic polymer, poly(diallyldimethylammonium chloride) (PDDA), on the films' physical properties (such as thickness and mass), structure, thermal stability, and flammability of cotton fabrics, PUF, and woods. Others have reported the effect of clays on FR performances, but relatively little work has been done on LbL deposition of dual clays and tris buffer, which imparts synergistically improved FR properties to the polymeric materials.[2,31−34] Incorporating amine salts into dual clay-based layers caused more clay nanoplatelets to be coated in the LbL processing steps. Introduction of tris buffer as a potential synergist in the dual clay-based multilayers promotes char formation, which provides a thermal shield to protect the underlying material. The best recipe was the PDDA-tris/VMT-MMT system, which completely eliminates the second peak HRR of PUF and shows a larger reduction in other FR parameters relative to the multilayer coatings made with no tris buffer. Both PUF and wood treated with only ten PDDA-tris/VMT-MMT bilayers retained structural integrity with no signs of melt dripping after direct exposure to a butane torch for 10 and 60 s, respectively.

EXPERIMENTAL SECTION

Materials and Substrates. PDDA (MW = 200,000−350,000 g/mol, 20 wt % aqueous solution), poly(acrylic acid) (PAA, MW = 1,000,000 g/mol, 35 wt % aqueous solution), VMT (batch Z765422), and tris(hydroxymethyl) aminomethane (tris, MW = 121.14 g/mol) buffer were purchased from Sigma-Aldrich (Milwaukee, WI). Natural sodium MMT (trade name Cloisite NA$^+$) was obtained from NANOCOR (Seoul, South Korea). The exfoliated VMT sheets were prepared by initially grinding 1 g of VMT powders in 1 wt % of MMT solutions using a mortar and pestle. Neat clay powders and their corresponding energy-dispersive X-ray (EDX) analyses indicated stacked platelet structures (Figure S1). The VMT-MMT mixtures in deionized (D.I) water with a resistance of 18.2 MΩ were bath sonicated for 30 min, followed by ultrasonication with a power of 45 W in an ice bath for 1 h, and another 30 min of bath sonication to ensure that the suspensions are completely homogenized. Bleached and desized cotton fabric (plain woven 100 g/m^2) was obtained from Testfabrics, Inc. (West Pittston, PA, USA). Single-side-polished silicon wafers (University wafer, South Boston, MA) and polished Ti/Au crystals of 5 MHz resonant frequency were used as deposition substrates to monitor the film growth behavior. A polyethylene terephthalate (PET) film with 188 μm thickness was provided from FilmBank (Gyeonggi-do, South Korea). Open-celled PUF (trade name: RJBB) was purchased from JeilDeco Systems (Seoul, South Korea) to assess flame-resistance behaviors.

https://doi.org/10.1021/acsomega.3c07534
ACS Omega 2024, 9, 6606−6615

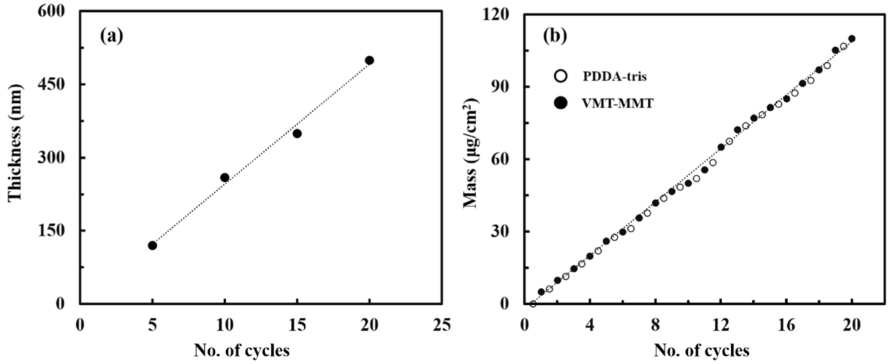

Figure 2. (a) Film thickness and (b) accumulated film mass as a function of deposited layers for PDDA-tris/VMT-MMT LbL thin films. Growth behavior of PDDA/MMT and PDDA/VMT-MMT systems is shown in the Supporting Information (Figure S1).

Film Deposition. The PDDA/MMT or PDDA/VMT-MMT LbL-based nanocomposites were prepared by alternately depositing cationic polyelectrolyte (0.25 wt % PDDA) and anionic suspensions of 1 wt % of MMT or VMT-MMT, respectively, on a given substrate by using a Multi Dip Coater robot (Hantech Co., Daejeon, South Korea) with rinsing steps of DI water three times for 1 min to eliminate weakly associated materials. Figure 1a,b shows schematics of the overall coating procedure, along with chemical structures used in this study. MMT was found to be very stable in water after stirring overnight (Figure 1c). Homogeneous dispersion of VMT in aqueous MMT was achieved after a pretreatment in the ultrasonic bath. Atomic force microscopy (AFM) images of MMT and VMT-MMT suspensions cast from dilute solutions indicated highly exfoliated particles, allowing for their successful deposition onto the substrates via LbL assembly. Initial dips into the positively charged PDDA and anionic mixture of clays were 5 min, followed by DI water rinsing for 1 min, with each cycle corresponding to one bilayer (BL). After the first BL was assembled, the rest of the subsequent dips were 1 min. The cycle was repeated until the BL reached the desired numbers. In the case of PDDA-tris/VMT-MMT assembly, the substrate was successively dipped into the polycation solution (50 mM tris was added in 0.25 wt % PDDA solution) for 5 min, subsequently dipping for 1 min in a solution with an equivalent concentration of tris buffer, then dipping into the VMT-MMT clay solution for 5 min, and finally rinsing with DI water for 1 min to complete 1 BL. After this initial BL was assembled, additional dips were for 1 min. The procedure for coating the polymer nanocomposites onto the fabrics and PUF was identical to that applied to the flat substrates (PET and Si-wafer) except that 2 wt % PAA, adjusted to pH 2, was deposited as a primer layer to enhance adhesion of each component onto three-dimensional structures. The cotton fabrics and PUF were rinsed with DI water for 1 min through wringing out by hand to eliminate the excessively adsorbed polymer chains.

Film Characterization. The film thickness of LbL assemblies deposited on Si-wafers was determined with a NanoMap-PS contact mode stylus profilometer (Aeptechnology, Santa Clara, USA). The mass of the films was analyzed on Ti/Au crystals using a quartz crystal microbalance (QCM) (Infinicon East Syracuse, NY), with a frequency range of 3.8−6. Weight gain is used as a measure of the amount of coating deposited on the fabric. Surface topography of clay-based polymer nanocomposites was visualized using an AFM (Nanostation IITM, Herzogenrath, Germany) in the non-contact mode at a scan rate of 1 Hz in the air. Top-view morphology of LbL assemblies was investigated by using a Hitachi S4700 Scanning Electron Microscope (SEM, Core Facility for Supporting Analysis & Imaging of Biomedical Materials at Wonkwang University supported by the National Research Facilities and Equipment Center) with the accelerating voltage of 20 kV. In order to prevent local charges, a thin layer of conductive material (platinum) was applied on the surface of the samples by sputter-coating. EDX analysis was performed by using an Oxford system micro-analyzer integrated with the SEM. Cross-sectional structures of clay-based polymer composites were captured using a JEMARM200F JEOL transmission electron microscope (TEM). The samples for these images were prepared by depositing them on a PET substrate and then employing the focused ion-beam technique, developed by the FEI Company in The Netherlands. X-ray diffraction (XRD) patterns of neat clay powders and LbL assemblies, deposited on Si-wafers, were obtained with a Japan D/MAX-2500 RUGAKU X-ray diffractometer at a step of 0.01° and a 2 s count time using Cu−Kα radiation (λ = 1.541 Å).

FR Characterization. The thermal behavior of the samples (approximately 20 mg) was examined on a Q-50 thermogravimetric analyzer (thermogravimetric analysis (TGA), TA Instruments, New Castle, DE) under a nitrogen atmosphere from room temperature to 700 °C at a heating rate of 5 °C/min. The fire-resistance behavior of square samples (100 mm × 100 mm size with a thickness of 10 mm) was investigated using a cone calorimeter (Fire Testing Technology, East Grinstead, UK) according to ISO 5660 standard procedures. Each specimen was exposed horizontally under a constant external heat flux (35 kW/m^2). Various FR parameters of uncoated and coated PUF samples were examined by a cone calorimeter: HRR, total heat release (THR), maximum average rate of heat emission (MARHE), total smoke release (TSP), effective heat of combustion (EHC), and total oxygen consumed (TOC). Vertical flame testing (VFT) was performed on five 50 × 100 mm^2 fabric samples according to ASTM D 6413. Horizontal flame testing (HFT) of the fabrics was performed according to the ASTM D5132 standard method. Wash durability was tested according to AATCC 135 by laundering with detergent in ambient conditions. The flame retardancy of PUF and woods was tested by subjecting the samples to the direct flame (≈1200 °C) of a butane hand torch to examine the fire-resistance characteristics of multilayered nanocomposites.

https://doi.org/10.1021/acsomega.3c07534
ACS Omega 2024, 9, 6606−6615

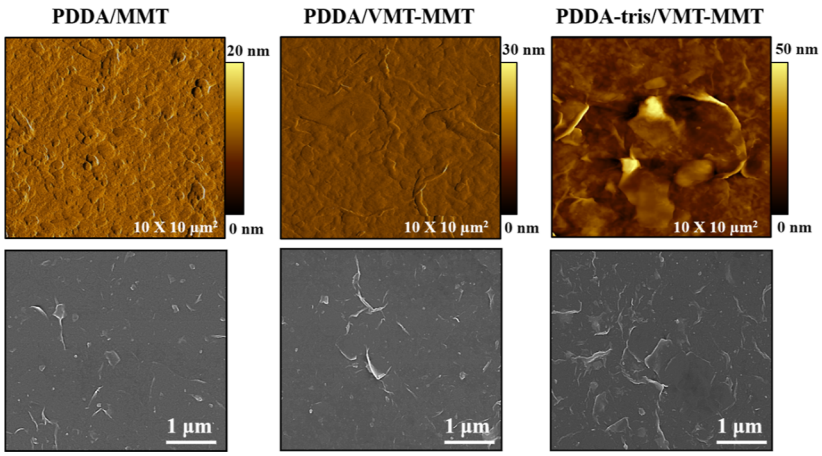

Figure 3. AFM height images (top row) and SEM surface structures (bottom row) of 20 BL PDDA/MMT, PDDA/VMT-MMT, and PDDA-tris/VMT-MMT thin films deposited on Si-wafers.

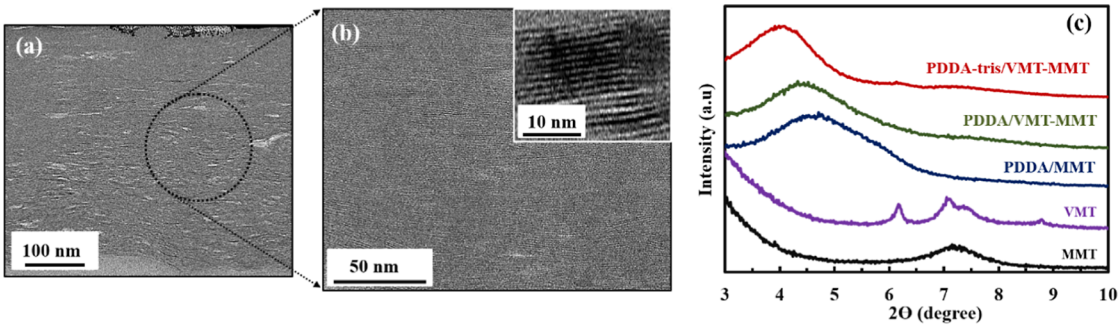

Figure 4. Cross-sectional TEM images of (a) 20 BL PDDA-tris/VMT-MMT assemblies deposited on PET substrates and a corresponding image with a high resolution (b). The inset reveals a nanobrick wall structure of these assemblies. XRD patterns (c) for neat MMT (black line), VMT (purple line), and LbL-assemblies coated with 100 BL PDDA/MMT (sky blue line), 60 BL PDDA/VMT-MMT (green line) and 20 BL PDDA-tris/VMT-MMT (red line) on Si-wafers. For interpretation of the references to color in this figure legend, the reader is referred to the web version of this article.

RESULTS AND DISCUSSION

Growth Behavior. The consecutive growth of three different PDDA/clay-based assemblies was monitored using a stylus profilometer. The reported thickness values were obtained by taking the average of five individual measurements conducted on three separate samples, resulting in 15 measurements in all. PDDA/MMT systems displayed a linear growth pattern as a function of the number of layers deposited, as shown in Figures 2a and S2a. The incorporation of VMT clays into PDDA/MMT films nearly doubled the thickness due to the higher aspect ratio of VMT platelets. The thickness of the PDDA/clay assembly increased further with the addition of tris buffer. PDDA-tris/VMT-MMT assemblies in which 50 mM tris buffer was added to the cationic PDDA solution grew at a much greater rate, with a 20 BL film achieving a thickness of 500 nm. The thickness of this system shows a 16.7 times increase in thickness/layer for the PDDA/MMT films and a 9.1 times increase for the PDDA/VMT-MMT films. As documented by previous studies, it has been theorized that alkylamines interact with the surface of clay sheets, leading to an extension of the gallery spacing between the clay platelets.[37−39] This could facilitate polymer intercalation between dispersed nanoclays, providing more interactive sites between the clay stacks. In this work, tris buffer, as a common amine salt, could interact with the clay platelets, inducing positively charged PDDA from the previously deposited layer to diffuse out between the nanoclays to the film's surface during deposition.[40−42] This attracts multiple stacks of the following layer (clay nanoparticles) to be deposited in order to satisfy the imparted surface charge, creating a thicker, more densely packed layer.

In order to further investigate this growth process, the weight increase of each individual layer in PDDA/clay assemblies was analyzed using a QCM. For film weight analysis, the mass increment for each individual layer was determined by conducting QCM measurements three times. When measured after each deposition step, the growth behavior in mass was similar to the linear trend observed with profilometry, with the growth rate of tris-buffered-added systems generating heavier layers (Figures 2b and S2b). As explained above, the introduction of tris buffer in the multilayer systems results in a thicker layer coating that would conceivably allow for more clay platelets during deposition. The film density was obtained by dividing the mass per unit area by its thickness. The density was calculated to be 1.46, 1.73, and 2.21 g/cm^3 for PDDA/MMT, PDDA/VMT-MMT, and PDDA-tris/VMT-MMT assemblies, respectively. A larger density in the PDDA-tris/VMT-MMT system suggests that more clay nanoplatelets were deposited efficiently in each dipping cycle.

Multilayer Structure. The surface morphology of clay-based multilayers was analyzed by using AFM and SEM. It is observed that all nanocomposites exhibited granular surface

https://doi.org/10.1021/acsomega.3c07534
ACS Omega 2024, 9, 6606−6615

structure, as shown in AFM images [Figure 3 (top row)]. The surface of 20 BL PDDA/MMT thin films was fully covered with MMT platelets visible in the range of 300−400 nm in diameter, while a larger grain structure appeared in the PDDA/VMT-MMT assemblies, which is most likely due to the incorporation of VMT sheets. The PDDA-tris/VMT-MMT multilayers displayed a rougher structure in the presence of tris buffer because of stronger interaction between clays and PDDA chains, as compared to the other two systems that had a relatively smooth surface. The SEM analysis further confirmed grain structures in MMT- and VMT-MMT-based thin films (Figure 3 (bottom row)). This granular surface became more prominent in the PDDA-tris/VMT-MMT nanocomposites. Some VMT particles were overlaid between the MMT layers. The surface of amine salt-added LbL assemblies exhibited a more densely packed clay structure. This observation is in good agreement with the film's growth behavior (thickness and mass increase) in which more clay particles are deposited in the presence of tris buffer during each deposition cycle relative to the other two systems.

A more detailed internal structure of clay-based nanocomposites was provided by TEM images. Figure 4a shows TEM cross sections of PDDA-tris/VMT-MMT multilayer thin films. The highly aligned platelets were clearly observed throughout a layered structure in which clay particles were found to be dark lines, while the PDDA appeared bright due to much lower electron density. Twenty BL PDDA-tris/VMT-MMT assemblies displayed many more clay platelets through the thickness of the film, which implies that clay sheets are deposited as multiplet stacks along the surface instead of being coated as one discrete layer (Figure 4b). It is interesting to note that the addition of tris buffer into the LbL systems caused more clay particles to be assembled during deposition without negatively affecting the formation of a uniformly layered structure. The inset image in Figure 4b emphasizes a nanobrick wall structure of these films with a high level of clay orientation. This unique nanostructure is expected to provide flame resistance to polymeric materials.

The multilayer structure and interlayer spacing of clay nanoplatelets were further investigated using an XRD scan (Figure 4c). The XRD pattern of neat MMT exhibited a (001) diffraction peak at $2\theta = 7.18^{\circ}$ which is assigned to the d_{001} of 1.23 nm.[43] The bare VMT powder displayed the specific diffraction peaks at $2\theta = 6.22^{\circ}$ (d = 1.42 nm), 7.12° (d = 1.24 nm), and 7.48° (d = 1.18 nm), indicating the presence of one or two water layer hydration states in the interstratified phases.[44−46] The reflection peak at 8.79° (d = 1.01 nm) can be attributed to the existence of mica phases.[47] Each diffraction peak of the raw organolay powders indicates the gallery spacing between the stacks of platelets. These characteristic peaks in the LbL assemblies were shifted to the smaller angles relative to those of bare clays, which increases the basal spacing; 2θ = 4.73, 4.48, and 4.05°, corresponding to the basal spacing = 1.87, 1.97, 2.18 nm for PDDA/MMT, PDDA/VMT-MMT, and PDDA-tris/VMT-MMT, respectively. The largest increment in *d*-spacing for the PDDA-tris/VMT-MMT system indicates higher spacing of layered platelets and a larger amount of PDDA intercalation between the clay sheets upon the addition of tris buffer. The broadening of XRD peaks in clay-based polymer nanocomposites compared to bare clay powders could be primarily due to the reduced crystallinity and altered structural arrangement caused by the interaction between the polymer and clays.

Thermal Stability. TGA was used to assess the thermal behavior by measuring the weight loss of a sample as a function of temperature. Figure 5 shows the thermal properties of clay

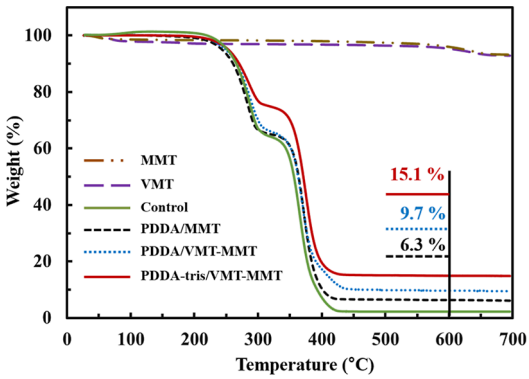

Figure 5. TGA curves of neat MMT and VMT powders and PUFs coated with 20 BL of PDDA/MMT, PDDA/VMT-MMT, and PDDA-tris/VMT-MMT thin films. Control refers to the uncoated PUF.

nanoparticles and 20 BL-coated PUF samples that were evaluated using TGA under a nitrogen atmosphere. Control PUF in the absence of an LbL coating began to degrade in the temperature range from 220 to 310 °C, which is closely related to the degradation of hard segments.[48,49] There was almost no residue left from the control PUF due to the pyrolysis of the remaining soft segments (polyol) when full degradation was reached near 420 °C. All coated PUF samples exhibited similar degradation curves to the uncoated sample, but PDDA-tris/VMT-MMT nanocomposites had higher mass. The final residues at 650 °C are 6.3, 9.7, and 15.1 wt % for PDDA/MMT, PDD/VMT-MMT, and PDDA-tris/VMT-MMT samples, respectively. This further confirms that the incorporation of tris buffer into the cationic polyelectrolyte solution increases the amount of clay platelets deposited on the surface, as compared to the multilayered nanocomposites made with no amine salts added. A higher amount of char residue achieved by incorporating amine salts into the dual clay-based coatings would be expected to improve the flame resistance of polymeric materials, as discussed in the next paragraph.

Flammability. The polymer/clay-based LbL nanocomposites were deposited onto cotton fabrics using the same general procedure as that assembled on silicon wafers and quartz crystals. Weight gain was calculated by weighing the fabric samples before and after coating treatment (Table S1). For each coating system, the weight gain was found to increase as the number of bilayers increased from 5 to 20. VFT was used to evaluate the FR properties of these coatings. The fabrics coated with 10 BL LbL assemblies exhibited FR behaviors with large amounts of residues, while the pristine cotton fabric was completely burned up the entire sample length, leaving no char at all, as shown in Figure 6 (top row). No particular differences were observed in these LbL-coated samples, demonstrating a highly efficient clay-based coating capable of protecting the fabrics from combustion.

Surface images of control and coated fabrics before and after VFT measurements were analyzed by using SEM. The control sample exhibited a smooth and clean surface with a few defects. An image of uncoated fabric after burning was omitted because they were completely consumed. Ten BL-coated fibers in each system prior to burning revealed a rough surface covered with

https://doi.org/10.1021/acsomega.3c07534
ACS Omega 2024, 9, 6606−6615

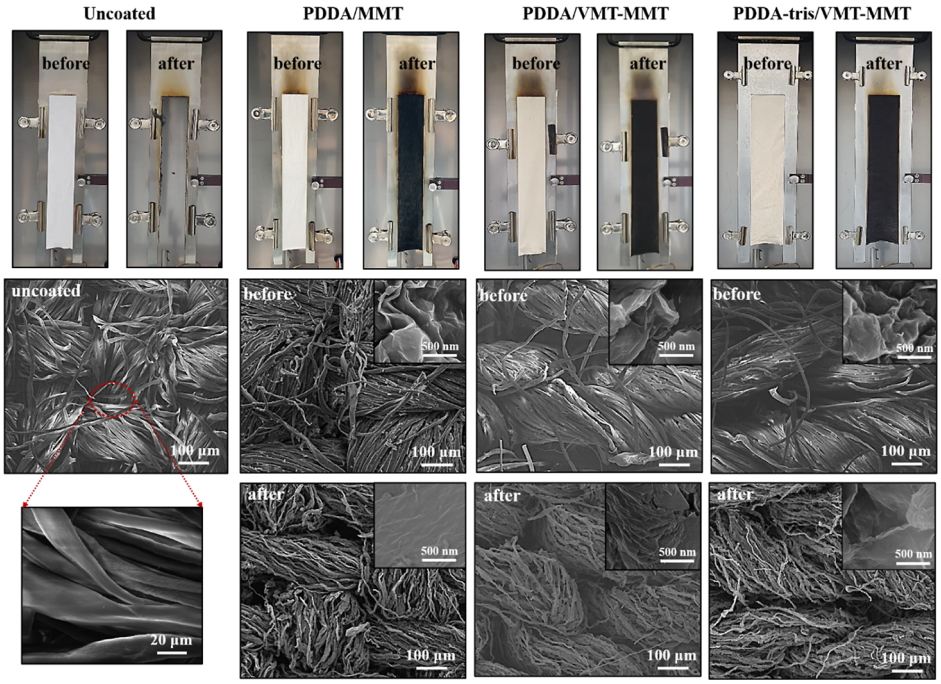

Figure 6. (Top row) vertical flame tests on coated and uncoated fabrics. SEM images of control and LbL-coated fabrics before (middle row) and after (bottom row) burning. The insets indicate clay platelets deposited onto each fiber.

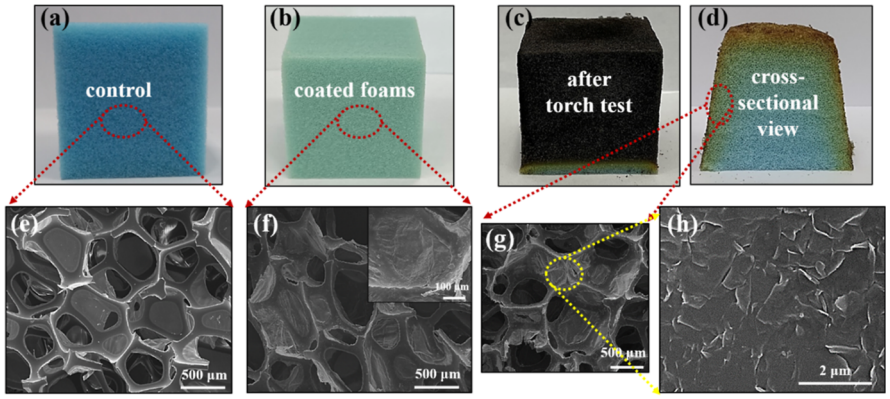

Figure 7. (Top row) Photo images (a–d) and (bottom row) SEM images (e–h) showing neat PUF and 10 BL PDDA-tris/VMT-MMT-coated PUF before and after torch tests, respectively. The inset image at high magnification shows a clay-based structure deposited on the foam surface.

thin layers of clay particles (Figure 6, middle row). The inset images at high magnification confirmed the presence of clay platelets coated on each individual fiber. This conformal coating on individual fibers highlights a homogeneous and continuous deposition of the LbL assembly. The weave structure of fabrics after burning was preserved, as shown in the bottom row of Figure 6. At higher magnification (inset images), some aggregated clay platelets being fused during burning were clearly observed. Horizontal burn testing further confirmed the FR performance of the multilayer nanocomposites. When the main flame passed through, the control fabric completely burned, leaving virtually no char (Figure S3). However, all coated fabrics left significant residue. The durability of fabrics during washing is a key factor, especially for polymeric materials treated with a protective coating. The LbL-based nanocomposites have demonstrated impressive water stability, primarily due to their strong ionic cross-linking.[32] Similar LbL coatings on textiles have demonstrated stability when exposed to boiling water and standard home laundry processes.[50] To assess wash durability, coated textile samples were subjected to five cycles of home laundering with detergent. Remarkably, fabrics coated with 10 BL PDDA-tris/VMT-MMT maintained the FR properties even after these wash cycles, as evidenced by both vertical and horizontal flame tests, leaving a substantial amount of residue (Figure S5). This highlights the high stability of the coating through repeated washing cycles, effectively maintaining its FR properties.

Foam flammability was tested by holding samples to the flame from a butane torch for 12 s. The PUF sample burned out in the absence of a coating and melted immediately upon flame exposure, leaving no residue (Video S1). 10BL PDDA/MMT or PDDA/VMT-MMT coating on PUF completely eliminated melt dripping, but both foams almost collapsed after the flame traveled across their surface (Videos S2 and S3). Ten BL PDDA-tris/VMT-MMT coating extinguished the flame and maintained the shape of the PUF during torch testing, leaving 75 wt % residue (Video S4). The surface structure studied using the photo image and SEM micrograph

https://doi.org/10.1021/acsomega.3c07534
ACS Omega 2024, 9, 6606−6615

of the neat PUF revealed a typical three-dimensional (3D) architecture with open cells connected to each other, as shown in Figure 7a,e. The 10 BL PDDA-tris/VMT-MMT coated foam showed excellent coverage of pore wall without any change in the macroscale porosity, and the high magnified inset image displayed a clay-coated surface structure, demonstrating a successful LbL deposition onto complex geometry-based substrates (Figure 7b,f). When cut through the middle of the torch-treated PUF with a razor blade, the foam was partially decomposed at the surface and appeared undamaged (green) underneath the char, maintaining 3D structures of the foam (Figure 7c,d,,g). The SEM observation of the burnt region (the interface between the black char and green foam) with a higher magnification revealed that the PUF sample is covered with aggregated clay platelets (Figure 7h). These results suggest that incorporating tris buffer into dual clay-based nanocomposites provides a more protective barrier due to enhanced char formation relative to the other two systems.

As for the practical application of this nanocoating system in industrial use, we coated 10 BL PDDA-tris/VMT-MMT nanocomposites onto wood and compared the FR performances with the control ones. The deposition procedure was performed by spraying-based coating in which 4 mm thick birch was vertically placed at a distance of 15 cm from the spray coater. Each component was sprayed for 20 s with no rinse steps. When the uncoated wood was exposed to the flame from a butane torch for 1 min, most of the birch was consumed after the flame died out (Figure S4 and Video S5). However, in the case of the coated wood, the glow disappeared in less than 2 s once the flame disappeared, maintaining its structure (Video S6). We believe that this halogen-free FR coating system can be utilized to protect buildings and offer powerful solutions for modern construction industry safety.

In order to quantitatively assess the inherent flammability of polymer/clay nanocomposites, cone calorimetry tests were carried out on 10 BL-coated LbL samples. The HRR, as an indicator of flammability, curves for PUF and coated PUF are shown in Figure 8 and the other important parameters obtained from the cone test, such as the THR, MARHE, TSP, EHC, and TOC are listed in Table S2. The control PUF displayed two major peaks in the HRR curve, both of which are related to the combustion of the decomposition products. A rapid rise to the first peak (245.7 kW/m^2) appeared at 5 s upon ignition, which implies that the foam sample has collapsed. Once its transformation to a liquid is completed, PUF burning is accelerated with the rapid vaporization of decomposed materials, which consequently results in a fast progression to a second, larger-peak HRR (380.3 kW/m^2). After being coated with 10 BL PDDA/MMT assemblies, the peak HRR (pkHRR) in the second peak was 267.1 kW/m^2 (reduction by 29.7%), but the first pkHRR was increased to 314.2 kW/m^2, which is larger relative to that of control PUF. This higher initial peak is believed due to the catalytic sites on clay surfaces.[51] When two inorganic particles cooperate (PDDA/VMT-MMT), the pkHRR (184.2 kW/m^2) represented a further reduction of 51.6%. It can be concluded that the incorporation of dual clays (MMT and VMT) imparts a more effective barrier to heat transfer than the polymer nanocomposites made by MMT alone. The 10 BL PDDA-tris/VMT-MMT nanocoating (≈250 nm thick) completely eliminated the second HRR peak, indicating that the addition of amine salts into a dual clay-based coating system greatly improves the FR properties because of enhanced char formation. A higher HRR observed in longer time zones in clay-based nanocomposites can be explained as follows; clay-based polymer composites used as FR coatings can slow down heat transfer from flames, delaying and increasing the HRR over time. Additionally, these composites help form a protective char layer on their surface, which insulates the material underneath from heat and flames, potentially causing an increase in HRR during its formation in a longer time frame. As expected, there was a visible improvement in other FR performances including THR, MARHE, TSR, EHC, and TOC by 12.8, 8.1, 58.1, 17.1, and 12.2%, respectively, in comparison with neat foam, each of which shows a greater reduction than those obtained from the MMT and VMT-MMT-based coatings.

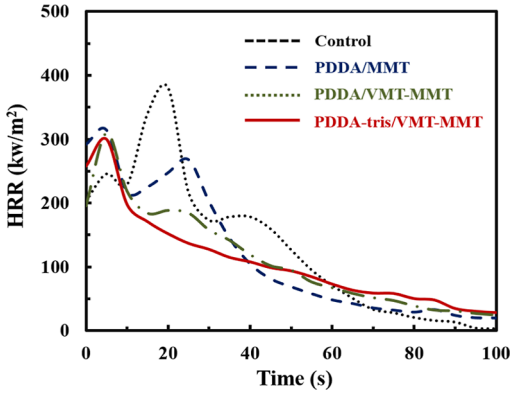

Figure 8. HRR, as a function of time, during cone calorimeter testing for uncoated control and 10 BL PDDA/MMT, PDDA/VMT-MMT, and PDDA-tris/VMT-MMT assemblies that are coated on PUF.

The present study demonstrates an efficient FR coating system with relatively few layers in which a single-digit-thick clay sheet is deposited into a highly oriented nanobrick wall structure. Thermal stability (TGA) and flame testing (VFT, HFT, torch tests, and cone calorimeter analysis) highlight the higher fire resistance of the PDDA-tris/VMT-MMT coatings. Inclusion of tris buffer into dual clay-based coatings creates a thicker layer per each assembly cycle with a larger amount of clay nanoplatelets deposited, which provides more effective thermal protection to the underlying polymeric substrate from heat. Clays are a passive FR, acting as an insulation barrier that protects the underlying materials from decomposing upon exposure to flame.[52] As reported in other clay-based LbL assemblies, this flame-retardant behavior is due to the ability of aggregated clay sheets on the surface of polymer nanocomposites that form an insulating layer, which dilutes gases in the flame.[53−55] When amine salts were included in the coating, more clays in each coating cycle were deposited, which led to the formation of high-density char during combustion. This strong char builds up a heat shield and diffusion barrier that effectively impede the transport of combustible gases.

CONCLUSIONS

This work demonstrates the incorporation of tris buffer in polymer/clay-based nanocomposites and its effectiveness in suppressing flames to various materials such as cotton fabrics, PUFs, and woods. The physical properties, such as thickness and mass, and the film's structure (analyzed by AFM, SEM, TEM, and XRD) demonstrated that this unique coating can be successfully constructed on various substrates. PDDA-tris/

https://doi.org/10.1021/acsomega.3c07534
ACS Omega 2024, 9, 6606−6615

VMT-MMT LbL assemblies exhibited thicker and heavier growth behavior relative to those of PDDA/MMT and PDDA/VMT-MMT systems. Clay-based polymer nanocomposites significantly reduced the flammability of fabrics during vertical and HFT. The addition of tris buffer to the PDDA solution is believed to be the key factor in enhancement of thermal stability and flame retardancy. The PUF coated with 10 BL PDDA-tris/VMT-MMT (≈250 nm in thickness) exhibited complete elimination of the second HRR peak, as measured by the cone calorimeter. Furthermore, this multilayer system in the presence of tris buffer further reduced other FR performances, including THR, MARHE, TSR, EHC, and TOC, compared to those obtained from the other two coating systems. Improved flame retardancy in PDDA-tris/VMT-MMT results from enhanced char formation upon the incorporation of amine salts into the multilayer structures. As evidenced by the film's growth behavior, XRD, and TEM, the presence of tris buffer in the multilayer coating induces more organoclays to be assembled without altering a highly ordered nanobrick wall structure. These halogen-free and industrially feasible (i.e., simple and low-cost) coatings, assembled via water-based chemistry under ambient conditions, could offer a new way to prepare excellent fire-resistant materials.

■ ASSOCIATED CONTENT

Supporting Information

The Supporting Information is available free of charge at https://pubs.acs.org/doi/10.1021/acsomega.3c07534.

SEM images of neat MMT and VMT powders and corresponding EDX analyses, film growth and mass of PDDA/MMT and PDDA/VMT-MMT, weight gains of each LbL system, horizontal flame tests on uncoated and coated fabrics, photo images of uncoated and coated woods, and FR behaviors obtained from a cone calorimeter analysis (PDF)

Video S1 (MP4)

Video S2 (MP4)

Video S3 (MP4)

Video S4 (MP4)

Video S5 (MP4)

Video S6 (MP4)

■ AUTHOR INFORMATION

Corresponding Authors

Ji Hyun Ryu − *Department of Carbon Convergence Engineering, College of Engineering, Wonkwang University, Iksan 54538, Republic of Korea;* orcid.org/0000-0002-0279-7477; Email: jhryu4816@wku.ac.kr

Dongwhi Choi − *Department of Mechanical Engineering, Kyung Hee University, Yongin-si, Gyeonggi-do 17104, Republic of Korea;* orcid.org/0000-0002-9286-2710; Email: dongwhi.choi@khu.ac.kr

Chungyeon Cho − *Department of Carbon Convergence Engineering, College of Engineering, Wonkwang University, Iksan 54538, Republic of Korea;* orcid.org/0000-0001-6689-8106; Email: cncho37@wku.ac.kr

Authors

Inyoung Lee − *Department of Carbon Convergence Engineering, College of Engineering, Wonkwang University, Iksan 54538, Republic of Korea*

Jinhong Kim − *Department of Carbon Convergence Engineering, College of Engineering, Wonkwang University, Iksan 54538, Republic of Korea*

Sehui Yun − *Department of Carbon Convergence Engineering, College of Engineering, Wonkwang University, Iksan 54538, Republic of Korea*

Junho Jang − *Wearable Platform Materials Technology Center (WMC), Department of Materials Science and Engineering, Korea Advanced Institute of Science and Technology (KAIST), Daejeon 34141, Republic of Korea*

Se Youn Cho − *Carbon Composite Materials Research Center, Korea Institute of Science and Technology, Wanju-gun, Jeonbuk 55324, Republic of Korea*

Jung Sang Cho − *Department of Engineering Chemistry, Chungbuk National University, Cheongju, Chungbuk 361-763, Republic of Korea*

Complete contact information is available at: https://pubs.acs.org/10.1021/acsomega.3c07534

Author Contributions

#I.L. and J.K. contributed equally to this study.

Notes

The authors declare no competing financial interest.

■ ACKNOWLEDGMENTS

This work was supported by the National Research Foundation of Korea (NRF) grant funded by the Korea government (MSIT) (no. NRF-2021R1F1A1049361). This research was also supported by "Regional Innovation Strategy (RIS)" through the National Research Foundation of Korea(NRF) funded by the Ministry of Education(MOE) (2023RIS-005)

■ REFERENCES

(1) Yang, H.; Yu, B.; Song, P.; Maluk, C.; Wang, H. Surface-coating engineering for flame retardant flexible polyurethane foams: A critical review. *Compos. B: Eng.* **2019**, *176*, 107185.

(2) Qiu, X.; Li, Z.; Li, X.; Zhang, Z. Flame retardant coatings prepared using layer by layer assembly: A review. *Chem. Eng. J.* **2018**, *334*, 108−122.

(3) Chung, Y.-j.; Kim, Y.; Kim, S. Flame retardant properties of polyurethane produced by the addition of phosphorous containing polyurethane oligomers (II). *J. Ind. Eng. Chem.* **2009**, *15* (6), 888−893.

(4) Popescu, C. M.; Pfriem, A. Treatments and modification to improve the reaction to fire of wood and wood based products—An overview. *Fire Mater.* **2020**, *44* (1), 100−111.

(5) Taib, M. N. A. M.; Antov, P.; Savov, V.; Fatriasari, W.; Madyaratri, E. W.; Wirawan, R.; Osvaldová, L. M.; Hua, L. S.; Ghani, M. A. A.; Edrus, S. S. A. O. A.; et al. Current progress of biopolymer-based flame retardant. *Polym. Degrad. Stab.* **2022**, *205*, 110153.

(6) Xu, D.; Wang, S.; Berglund, L. A.; Zhou, Q. Surface charges control the structure and properties of layered nanocomposite of cellulose nanofibrils and clay platelets. *ACS Appl. Mater. Interfaces* **2021**, *13* (3), 4463−4472.

(7) Su, X.; Ma, L.; Wei, J.; Zhu, R. Structure and thermal stability of organo-vermiculite. *Appl. Clay Sci.* **2016**, *132*−*133*, 261−266.

(8) Kotal, M.; Bhowmick, A. K. Polymer nanocomposites from modified clays: Recent advances and challenges. *Prog. Polym. Sci.* **2015**, *51*, 127−187.

(9) Lee, S.; Yoo, J.; Lee, J. W. Water-assisted extrusion of polypropylene/clay nanocomposites in high shear condition. *J. Ind. Eng. Chem.* **2015**, *31*, 317−322.

(10) Weldemhret, T. G.; Menge, H. G.; Lee, D.-W.; Park, H.; Lee, J.; Song, J. I.; Park, Y. T. Facile deposition of environmentally benign

organic-inorganic flame retardant coatings to protect flammable foam. *Prog. Org. Coat.* **2021**, *161*, 106480.
(11) Patra, D.; Vangal, P.; Cain, A. A.; Cho, C.; Regev, O.; Grunlan, J. C. Inorganic nanoparticle thin film that suppresses flammability of polyurethane with only a single electrostatically-assembled bilayer. *ACS Appl. Mater. Interfaces* **2014**, *6* (19), 16903−16908.
(12) Tasdelen, M. A.; Kreutzer, J.; Yagci, Y. In situ synthesis of polymer/clay nanocomposites by living and controlled/living polymerization. *Macromol. Chem. Phys.* **2010**, *211* (3), 279−285.
(13) Pavlidou, S.; Papaspyrides, C. A review on polymer-layered silicate nanocomposites. *Prog. Polym. Sci.* **2008**, *33* (12), 1119−1198.
(14) Das, P.; Manna, S.; Behera, A. K.; Shee, M.; Basak, P.; Sharma, A. K. Current synthesis and characterization techniques for clay-based polymer nano-composites and its biomedical applications: A review. *Environ. Res.* **2022**, *212*, 113534.
(15) Richardson, J. J.; Cui, J.; Bjornmalm, M.; Braunger, J. A.; Ejima, H.; Caruso, F. Innovation in layer-by-layer assembly. *Chem. Rev.* **2016**, *116* (23), 14828−14867.
(16) Kang, K.; Lee, K.-H.; Han, Y.; Gao, H.; Xie, S.; Muller, D. A.; Park, J. Layer-by-layer assembly of two-dimensional materials into wafer-scale heterostructures. *Nature* **2017**, *550* (7675), 229−233.
(17) Zhao, S.; Caruso, F.; Dähne, L.; Decher, G.; De Geest, B. G.; Fan, J.; Feliu, N.; Gogotsi, Y.; Hammond, P. T.; Hersam, M. C.; et al. The future of layer-by-layer assembly: a tribute to ACS nano associate editor Helmuth Mohwald. *ACS Nano* **2019**, *13* (6), 6151−6169.
(18) Jung, S.; Park, S.; Choi, W.; Heo, J.; Kwon, J.; Choi, S.; Hong, J. Organosilicate compound filler to increase the mechanical strength of superhydrophilic layer-by-layer assembled film. *J. Ind. Eng. Chem.* **2020**, *84*, 332−339.
(19) Elizarova, I. S.; Luckham, P. F. Layer-by-layer adsorption: Factors affecting the choice of substrates and polymers. *Adv. Colloid Interface Sci.* **2018**, *262*, 1−20.
(20) Cho, C.; Xiang, F.; Wallace, K. L.; Grunlan, J. C. Combined ionic and hydrogen bonding in polymer multilayer thin film for high gas barrier and stretchiness. *Macromolecules* **2015**, *48* (16), 5723−5729.
(21) Forsman, N.; Lozhechnikova, A.; Khakalo, A.; Johansson, L.-S.; Vartiainen, J.; Österberg, M. Layer-by-layer assembled hydrophobic coatings for cellulose nanofibril films and textiles, made of polylysine and natural wax particles. *Carbohydr. Polym.* **2017**, *173*, 392−402.
(22) Ogoshi, T.; Takashima, S.; Yamagishi, T.-a. Molecular recognition with microporous multilayer films prepared by layer-by-layer assembly of pillar [5] arenes. *J. Am. Chem. Soc.* **2015**, *137* (34), 10962−10964.
(23) Schoeler, B.; Poptoshev, E.; Caruso, F. Growth of multilayer films of fixed and variable charge density polyelectrolytes: effect of mutual charge and secondary interactions. *Macromolecules* **2003**, *36* (14), 5258−5264.
(24) Wong, J. E.; Díez-Pascual, A. M.; Richtering, W. Layer-by-Layer assembly of polyelectrolyte multilayers on thermoresponsive P (NiPAM-co-MAA) microgel: Effect of ionic strength and molecular weight. *Macromolecules* **2009**, *42* (4), 1229−1238.
(25) Yuan, W.; Weng, G.-M.; Lipton, J.; Li, C. M.; Van Tassel, P. R.; Taylor, A. D. Weak polyelectrolyte-based multilayers via layer-by-layer assembly: Approaches, properties, and applications. *Adv. Colloid Interface Sci.* **2020**, *282*, 102200.
(26) Xiao, F.-X.; Pagliaro, M.; Xu, Y.-J.; Liu, B. Layer-by-layer assembly of versatile nanoarchitectures with diverse dimensionality: a new perspective for rational construction of multilayer assemblies. *Chem. Soc. Rev.* **2016**, *45* (11), 3088−3121.
(27) Vaterrodt, A.; Thallinger, B.; Daumann, K.; Koch, D.; Guebitz, G. M.; Ulbricht, M. Antifouling and antibacterial multifunctional polyzwitterion/enzyme coating on silicone catheter material prepared by electrostatic layer-by-layer assembly. *Langmuir* **2016**, *32* (5), 1347−1359.
(28) Lee, Y.-L.; Lin, T.-X.; Hsu, F.-M.; Jan, J.-S. Synthesis of antireflective silica coatings through the synergy of polypeptide layer-by-layer assemblies and biomineralization. *Nanoscale* **2016**, *8* (4), 2367−2377.
(29) Rydzek, G.; Ji, Q.; Li, M.; Schaaf, P.; Hill, J. P.; Boulmedais, F.; Ariga, K. Electrochemical nanoarchitectonics and layer-by-layer assembly: From basics to future. *Nano Today* **2015**, *10* (2), 138−167.
(30) Cho, C.; Song, Y.; Allen, R.; Wallace, K. L.; Grunlan, J. C. Stretchable electrically conductive and high gas barrier nanocomposites. *J. Mater. Chem. C* **2018**, *6* (8), 2095−2104.
(31) Holder, K. M.; Smith, R. J.; Grunlan, J. C. A review of flame retardant nanocoatings prepared using layer-by-layer assembly of polyelectrolytes. *J. Mater. Sci.* **2017**, *52* (22), 12923−12959.
(32) Lee, I.; Kim, S. J.; Byun, Y. Y.; Chang, I.; Ju, Y.-W.; Park, Y. T.; Jang, J.; Cho, C. High flame retardancy enabled by dual clays-based multilayer nanocomposites. *Prog. Org. Coat.* **2023**, *183*, 107784.
(33) Huang, G.; Liang, H.; Wang, X.; Gao, J. Poly (acrylic acid)/clay thin films assembled by layer-by-layer deposition for improving the flame retardancy properties of cotton. *Ind. Eng. Chem. Res.* **2012**, *51* (38), 12299−12309.
(34) Apaydin, K.; Laachachi, A.; Ball, V.; Jimenez, M.; Bourbigot, S.; Toniazzo, V.; Ruch, D. Polyallylamine-montmorillonite as super flame retardant coating assemblies by layer-by layer deposition on polyamide. *Polym. Degrad. Stab.* **2013**, *98* (2), 627−634.
(35) Priolo, M. A.; Holder, K. M.; Guin, T.; Grunlan, J. C. Recent Advances in Gas Barrier Thin Films via Layer-by-Layer Assembly of Polymers and Platelets. *Macromol. Mater. Eng.* **2015**, *36*, 866−879.
(36) Long, C. T.; Grunlan, J. C. Small molecule additives in multilayer polymer-clay thin films for improved heat shielding of steel. *npj Mater. Degrad.* **2022**, *6*, 22.
(37) Guin, T.; Krecker, M.; Hagen, D. A.; Grunlan, J. C. Thick growing multilayer nanobrick wall thin films: super gas barrier with very few layers. *Langmuir* **2014**, *30* (24), 7057−7060.
(38) Guin, T.; Krecker, M.; Milhorn, A.; Hagen, D. A.; Stevens, B.; Grunlan, J. C. Exceptional flame resistance and gas barrier with thick multilayer nanobrick wall thin films. *Adv. Mater. Technol.* **2015**, *2* (11), 1500214.
(39) Geng, F.; Ma, R.; Ebina, Y.; Yamauchi, Y.; Miyamoto, N.; Sasaki, T. Gigantic swelling of inorganic layered materials: A bridge to molecularly thin two-dimensional nanosheets. *J. Am. Chem. Soc.* **2014**, *136* (14), 5491−5500.
(40) Tertre, E.; Delville, A.; Prêt, D.; Hubert, F.; Ferrage, E. Cation diffusion in the interlayer space of swelling clay minerals-A combined macroscopic and microscopic study. *Geochim. Cosmochim. Acta* **2015**, *149*, 251−267.
(41) Lin, J.-J.; Wei, J.-C.; Juang, T.-Y.; Tsai, W.-C. Preparation of protein- silicate hybrids from polyamine intercalation of layered montmorillonite. *Langmuir* **2007**, *23* (4), 1995−1999.
(42) Le Pluart, L.; Duchet, J.; Sautereau, H.; Gérard, J. F. Surface modifications of montmorillonite for tailored interfaces in nanocomposites. *J. Adhes.* **2002**, *78* (7), 645−662.
(43) Kim, J.; Jang, J.; Yun, S.; Kim, H. D.; Byun, Y. Y.; Park, Y. T.; Song, J. I.; Cho, C. Synergistic Flame Retardant Effects of Carbon Nanotube-Based Multilayer Nanocoatings. *Macromol. Mater. Eng.* **2021**, *306* (9), 2100233.
(44) Janica, I.; Del Buffa, S.; Mikołajczak, A.; Eredia, M.; Pakulski, D.; Ciesielski, A.; Samorì, P. Thermal insulation with 2D materials: liquid phase exfoliated vermiculite functional nanosheets. *Nanoscale* **2018**, *10* (48), 23182−23190.
(45) Chen, J.; Xiang, L. Controllable synthesis of calcium carbonate polymorphs at different temperatures. *Powder Technol.* **2009**, *189* (1), 64−69.
(46) Anichini, C.; Czepa, W.; Pakulski, D.; Aliprandi, A.; Ciesielski, A.; Samorì, P. Chemical sensing with 2D materials. *Chem. Soc. Rev.* **2018**, *47* (13), 4860−4908.
(47) Muiambo, H. F.; Focke, W. W.; Atanasova, M.; der Westhuizen, I. v.; Tiedt, L. R. Thermal properties of sodium-exchanged palabora vermiculite. *Appl. Clay Sci.* **2010**, *50* (1), 51−57.
(48) Krämer, R.; Zammarano, M.; Linteris, G. T.; Gedde, U. W.; Gilman, J. W. Heat release and structural collapse of flexible polyurethane foam. *Polym. Degrad. Stab.* **2010**, *95* (6), 1115−1122.

https://doi.org/10.1021/acsomega.3c07534
ACS Omega 2024, 9, 6606−6615

(49) Lage, L. G.; Kawano, Y. Thermal degradation of biomedical polyurethanes—A kinetic study using high-resolution thermogravimetry. *J. Appl. Polym. Sci.* **2001**, *79* (5), 910−919.
(50) Kundu, C. K.; Hossen, M. T.; Islam, T.; Mollick, S.; Song, L.; Hu, Y. Flame Retardant Coatings from Bio-Derived Chitosan, Sodium Alginate, and Metal Salts for Polyamide 66 Textiles. *ACS Omega* **2022**, *7*, 30841−30848.
(51) Zanetti, M.; Kashiwagi, T.; Falqui, L.; Camino, G. Cone calorimeter combustion and gasification studies of polymer layered silicate nanocomposites. *Chem. Mater.* **2002**, *14* (2), 881−887.
(52) Haile, M.; Fomete, S.; Lopez, I. D.; Grunlan, J. C. Aluminum hydroxide multilayer assembly capable of extinguishing flame on polyurethane foam. *J. Mater. Sci.* **2016**, *51*, 375−381.
(53) Liu, Q.; Gao, S.; Zhao, Y.; Tao, W.; Yu, X.; Zhi, M. Review of layer-by-layer self-assembly technology for fire protection of flexible polyurethane foam. *J. Mater. Sci.* **2021**, *56*, 9605−9643.
(54) Lazar, S. T.; Kolibaba, T. J.; Grunlan, J. C. Flame-retardant surface treatments. *Nat. Rev. Mater.* **2020**, *5* (4), 259−275.
(55) Wen, O. Y.; Tohir, M. Z. M.; Yeaw, T. C. S.; Razak, M. A.; Zainuddin, H. S.; Hamid, M. R. A. Fire-resistant and flame-retardant surface finishing of polymers and textiles: A state-of-the-art review. *Prog. Org. Coat.* **2023**, *175*, 107330.

https://doi.org/10.1021/acsomega.3c07534
ACS Omega 2024, 9, 6606−6615